Precise alignment of off-axis three-mirror reflecting optical system based on phase diversity

Qiang Cheng (程 强)

Changchun Institute of Optics, Fine Mechanics and Physics, Chinese Academy of Sciences, Changchun 130033, China

Corresponding author: nklance@gmail.com

Received April 22, 2014; accepted July 16, 2014; posted online January 26, 2015

Phase diversity (PD) is a kind of wavefront sensing technology based on image collecting and post-processing. We apply the PD technology to align an off-axis three-mirror reflecting anastigmatic system precisely. It can be concluded that the wavefront error obtained by PD agrees well with the interferometric result. The focused images are also restored according to the testing results of PD, and the qualities of restored images are improved.

OCIS codes: 100.5070, 010.7350, 100.3020, 110.6770.

doi: 10.3788/COL201513.S11003.

Phase diversity (PD) is a kind of wavefront sensing technology based on image collecting and post-processing. Because of its low cost, optically simple wavefront sensing, and its concise optical layout, it is widely used in optical wavefront testing and image restoration[1,2]. Furthermore, the PD technology works well with either point objects or extended objects. The PD technology requires two images during the wavefront testing: one is in focus which suffers from the unknown wavefront error of the system and the other is diversity image which contains certain designed aberration. Customarily, defocus is introduced to be the additional aberration for simplicity as shown in Fig. 1[3]. The computation of wavefront error from the two images can be concluded as an optimization problem mathematically and the maximum-likelihood theorem can be applied to deal with the problem, which was initially expatiated by Gonsalves *et al.*[4,5].

When the object is illuminated by spatially incoherent and quasi-monochromatic light, the imaging system is regarded as linear shift-invariant system. And the imaging equation of the optical system can be written as

$$i_k(x,y) = o(x,y) * \mathrm{PSF}_k(x,y) + n_k(x,y), \quad k = 1,2, \tag{1}$$

where k denotes the number of channels, i_k is the image collected by the detector of the kth channel, o is the ideal object image, PSF_k is the point-spread function of the kth channel, n_k denotes the additive Gaussian noise of the kth channel, $*$ represents 2D convolution, and x, y denote the coordinates of image plane.

According to the Parseval theorem, Eq. (1) can be expressed in frequency domain as

$$I_k(u,v) = O(u,v) \bullet \mathrm{OTF}_k(u,v) + N_k(u,v), \quad k = 1,2, \tag{2}$$

where I_k, O, OTF_k, and N_k are the Fourier transform of i_k, o, PSF_k and n_k, respectively.

The PSF can be obtained by performing Fourier transform on the pupil function as

$$\mathrm{PSF}_1 = \left| F\left\{ A(x,y) \exp\left[\mathrm{i}\phi(x,y) \right] \right\} \right|^2, \tag{3}$$

$$\mathrm{PSF}_2 = \left| F\left\{ A(x,y) \exp\left\{ \mathrm{i}\left[\phi(x,y) + \phi_d(x,y) \right] \right\} \right\} \right|^2, \tag{4}$$

and the phase function is expanded on a set of Zernike polynomials. Indeed, aberration in an optical system which can be mathematically represented by Zernike polynomials as

$$\phi(x,y) = \sum_{i=1}^{K} a_i Z_i(\rho,\theta), \tag{5}$$

$$\phi_{\mathrm{d}}(x,y) = a_4 Z_4(\rho,\theta), \tag{6}$$

where A denotes the binary aperture function, ϕ is the unknown pupil function, ϕ_{d} is the additional diversity function, K is the number of Zernike polynomials, Z_i is the ith Zernike polynomial, and a_i is the ith Zernike coefficient. Theoretically, K should tend to infinity to describe any waveform, but in our case of static aberration estimation, the first nine polynomials are enough to describe the aberrations.

According to the maximum-likelihood theory, after some mathematical processes, the final form of merit function is shown as

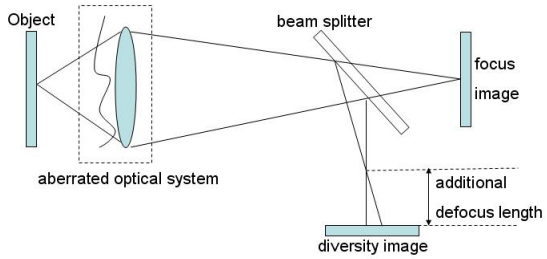

Fig. 1. Optical layout of PD.

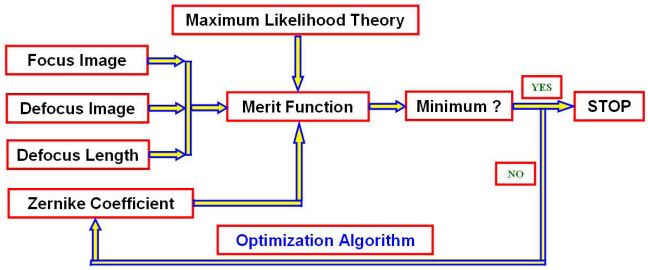

Fig. 2. Flow chart of PD technology.

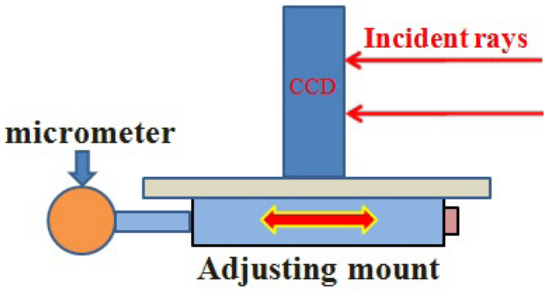

Fig. 4. Schematic of imaging equipment.

$$E(u,a)=\frac{1}{2}\left(\sum_{u\in X}\left(\left|I(u)\right|^2+\left|I_d(u)\right|^2-\left|\frac{I^*(u)\mathrm{OTF}_\mathrm{d}(u)-I_\mathrm{d}{}^*(u)\mathrm{OTF}(u)}{\gamma+\left|\mathrm{OTF}(u)\right|^2+\left|\mathrm{OTF}_\mathrm{d}(u)\right|^2}\right|^2\right)\right), \tag{7}$$

where γ is the nonnegative coefficient of regular term, and it can improve the stability and convergence efficiency of the algorithm. When E in Eq. (7) reaches its minimum value, the solved OTF will agree with its actual OTF, and the coefficients of Zernike polynomials can be solved. Thus, the wavefront of system can be fitted. The flow chart of PD algorithm is shown in Fig. 2. According to the aforementioned theory and algorithm, the adaptability analysis of PD technology is accomplished[6].

We have applied PD technology to align an off-axis three-mirror reflecting anastigmatic (TMA) system precisely[7,8]. The experimental setup is shown in Fig. 3.

An integrating sphere is applied as the light source, and a filter centered at 645.32 nm is used. The resolution target is illuminated as an infinite object. The F number ($F^{\#}$) of optical system is 9.83. The camera is FL2-20S4M-C charge-coupled device (CCD; Point Grey Corp.), the effective pixel number is 1600×1200 and its single pixel size is 4.4×4.4 (μm). The CCD camera is located on a 6D adjusting mount. Furthermore, the designed defocus is introduced by moving the CCD along the direction of the incident chief ray and a micrometer is used to monitor the defocus distance as shown in Fig. 4.

The initial position of the CCD is decided in alignment, where the actual defocus W020 of the optical system is practically zero. This initial position can also be regarded as the nominal ideal image plane.

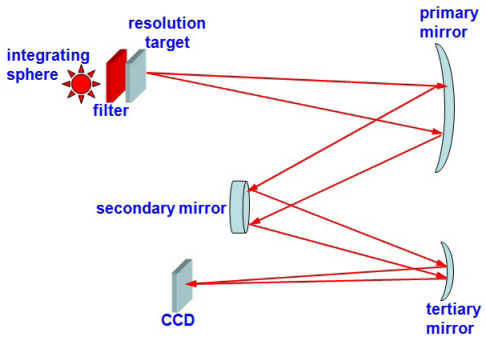

Fig. 3. Experimental setup of precise alignment.

According to the coarse-aligned TMA optical system, two images are collected: one image is in focus and the other is diversity image whose defocus distance is four times the depth of focus, that is, 0.499 mm. The same areas of 128×128 (pixel) of both images are clipped from the original images for simplicity. In order to verify the result of PD technology, the interferometric testing of the system is also carried out and its measured data are set as the criterion. It can be concluded from the comparison as shown in Table 1 and Fig. 5 that the result solved by PD technology agrees well with the interferometric testing.

The root-mean-square (RMS) value of the wavefront error solved by PD technology as shown in Fig. 6(a) is 0.317λ while the interferometric result as shown in Fig. 6(b) is 0.319λ. The testing error of PD technology is 0.0325λ. It can be seen that the main characters of the two wavefront error maps coincide with each other. It should also be pointed out that the more detailed wavefront error of high spatial frequency is lost in PD processing because the terms of Zernike polynomials are limited.

Table 1. Comparison of Zernike Coefficients by Two Methods (Coarse-aligned)

Zernike Item	PD/λ	Interferometer/λ	Deviation/λ
5	−0.0342	−0.0038	−0.0304
6	0.0274	0.010	0.0174
7	0.4032	0.4381	−0.0349
8	−0.3965	−0.4426	0.0461
9	−0.0171	−0.0313	0.0142
10	0.4997	0.4504	0.0493
11	0.4835	0.4655	0.018

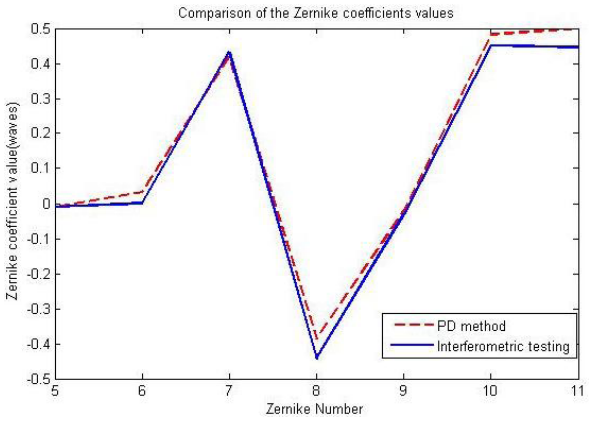

Fig. 5. Comparison of the Zernike coefficients obtained by two methods.

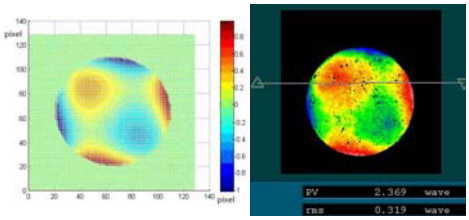

(a) (b)

Fig. 6. Comparison of wavefront map obtained by two methods (coarse-aligned): (a) PD technology and (b) interferometer.

According to the testing result of coarse-aligned optical system obtained by PD technology, the TMA system is precisely aligned further. The images of different fields of view are collected, and the wavefront aberration of several fields of view is solved by PD technology. In the same way, the interferometric testing is applied to test the wavefront aberration of the above fields of view. The comparisons of the wavefront maps obtained by two methods are shown in Figs. 7–9.

The RMS values of different fields of view obtained by PD technology are 0.0715λ, 0.0682λ, and 0.0703λ, and the testing errors of PD are all less than 0.02λ. The images are also restored by the Lucy–Richardson filter algorithm based on the results obtained by PD and they are compared with the original focused images (Fig. 10).

It can be seen that both the contrast and the definition of the restored images improve compared

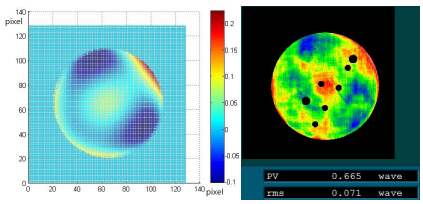

(a) (b)

Fig. 7. Comparison of wavefront map of +1 field of view obtained by two methods (precisely aligned): (a) PD technology and (b) interferometer.

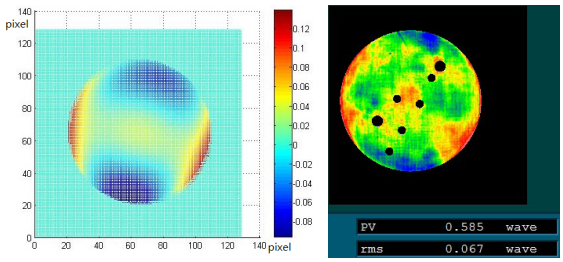

(a) (b)

Fig. 8. Comparison of wavefront map of 0 field of view obtained by two methods (precisely aligned): (a) PD technology and (b) interferometer.

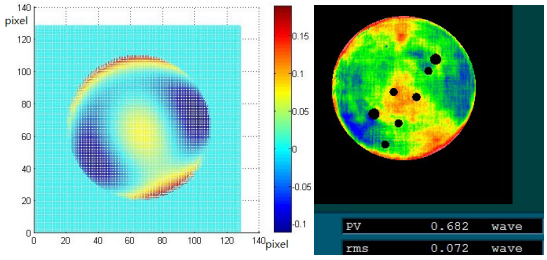

(a) (b)

Fig. 9. Comparison of wavefront map of −1 field of view obtained by two methods (precisely aligned): (a) PD technology and (b) interferometer.

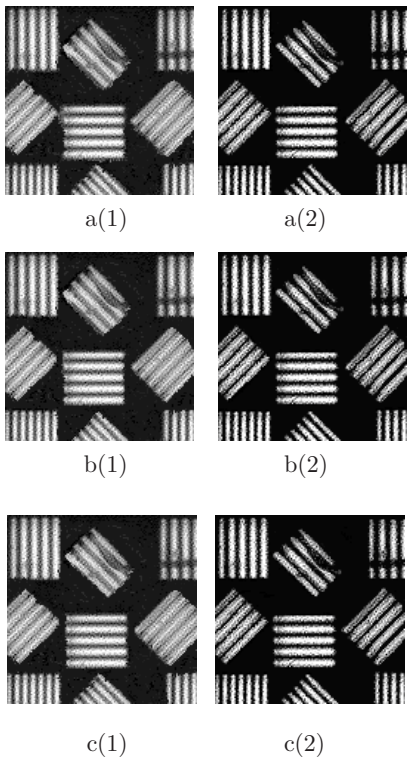

a(1) a(2)

b(1) b(2)

c(1) c(2)

Fig. 10. Collected focused images and restored images when the TMA optical system is precisely aligned: (a(1)–a(2)) focus image and restored image of +1 field of view, (b(1)–b(2)) focus image and restored image of 0 field of view, and (c(1)–c(2)) focus image and restored image of −1 field of view.

Table 2. RMSE and LS Values of Different Images When System is Precisely Aligned

Field of View	Evaluation Function	Focus Image	Restored Image
+1	RMSE	79.34	95.35
	LS	162.47	220.35
0	RMSE	81.54	99.81
	LS	165.61	228.62
−1	RMSE	79.13	94.86
	LS	159.07	224.39

with the original images. Also, the RMS error (RMSE) and Laplacian sum (LS) are applied to estimate the quality of the images as shown in Table 2. The definitions of RMSE and LS are shown as

$$\mathrm{RMSE} = \sqrt{\frac{1}{MN}\sum_{i=0}^{M-1}\sum_{j=0}^{N-1}\left[f(i,j) - f_{\mathrm{mean}}\right]^2}, \tag{8}$$

$$\mathrm{LS} = \frac{\sum_{i=2}^{M-1}\sum_{j=2}^{N-1}\left|9f(i,j) - \sum_{i=i-1}^{i+1}\sum_{j=j-1}^{j+1} f(i,j)\right|}{(M-2)(N-2)}. \tag{9}$$

In conclusion, we apply the PD technology to align the TMA optical system precisely. When the system is aligned well, the testing results of all fields of view by PD technology agrees well with the interferometric results. The deviations between the wavefront errors obtained by PD testing and by interferometric testing are all less than 0.02λ (RMS). The future work includes accelerating the mathematical calculation and the PD technology with the broadband light illumination.

This work was supported by State Key Program of National Natural Science Foundation of China (No. 61036015) and the 973 Project (No. O8663NJ090).

References

1. R. G. Paxman, B. J. Thelen, R. J. Murphy, K. W. Gleichman, and J. A. Georges III, Proc. SPIE **6711,** 671103 (2007).
2. J. A. Georges III, P. Dorrance, K. Gleichman, J. Jonik, D. Liskow, H. Lapprich, V. Naik, S. Parker, R. Paxman, M. Warmuth, A. Wilson, and T. Zaugg, Proc. SPIE **6711,** 671106 (2007).
3. D. J. Lee, M. C. Roggemann, B. M. Welsh, E. R. Crosby, Appl. Opt. **36,** 9186 (1997).
4. R. A. Gonsalves and R. Chidlaw, Proc. SPIE **207,** 32 (1997).
5. R. G. Paxman and J. R. Fienup, J. Opt. Soc. Am. A **5,** 914 (1988).
6. Q. Cheng, "The research on phase retrieval in space-borne camera based on phase diversity," PhD. Thesis (University of Chinese Academy of Sciences, 2013).
7. Q. Cheng, F. Li, X. Tao, F. Yan, and X. Zhang, Proc. SPIE **8417,** 84170R (2012).
8. Q. Cheng, F. Yan, D. Xue, L. Zheng, and X. Zhang, Chin. J. Lasers **39,** 1008001 (2012).